Theoretical investigation on radiation tolerance of $M_{n+1}AX_n$ phases*

Ke-Di Yin(殷克迪)[1,†], Xi-Tong Zhang(张西通)[1,†], Qing Huang(黄庆)[3], and Jian-Ming Xue(薛建明)[1,2,‡]

[1] State Key Laboratory of Nuclear Physics and Technology, School of Physics, Peking University, Beijing 100871, China
[2] CAPT, HEDPS, and IFSA Collaborative Innovation Center of MoE College of Engineering, Peking University, Beijing 100871, China
[3] Ningbo Institute of Material Technology and Engineering, Chinese Academy of Sciences, Ningbo 315201, China

(Received 22 November 2016; revised manuscript received 10 March 2017; published online 20 April 2017)

Ternary $M_{n+1}AX_n$ phases with layered hexagonal structures, as candidate materials used for next-generation nuclear reactors, have shown great potential in tolerating radiation damage due to their unique combination of ceramic and metallic properties. However, $M_{n+1}AX_n$ materials behave differently in amorphization when exposed to energetic neutron and ion irradiations in experiment. We first analyze the irradiation tolerances of different $M_{n+1}AX_n$ (MAX) phases in terms of electronic structure, including the density of states (DOS) and charge density map. Then a new method based on the Bader analysis with the first-principle calculation is used to estimate the stabilities of MAX phases under irradiation. Our calculations show that the substitution of Cr/V/Ta/Nb by Ti and Si/Ge/Ga by Al can increase the ionicities of the bonds, thus strengthening the radiation tolerance. It is also shown that there is no obvious difference in radiation tolerance between $M_{n+1}AC_n$ and $M_{n+1}AN_n$ due to the similar charge transfer values of C and N atoms. In addition, the improved radiation tolerance from Ti_3AlC_2 to Ti_2AlC (Ti_3AlC_2 and Ti_2AlC have the same chemical elements), can be understood in terms of the increased Al/TiC layer ratio. Criteria based on the quantified charge transfer can be further used to explore other $M_{n+1}AX_n$ phases with respect to their radiation tolerance, playing a critical role in choosing appropriate MAX phases before they are subjected to irradiation in experimental test for future nuclear reactors.

Keywords: MAX phases, radiation tolerance, Bader analysis, the first principle calculation

PACS: 07.05.Wr, 28.41.Qb, 47.54.Jk **DOI:** 10.1088/1674-1056/26/6/060703

1. Introduction

$M_{n+1}AX_n$ (M: an early transition metal, A: group III or IV element, and X: C or N) phase materials have attracted considerable attention for their best attributes of both ceramics and metals.[1] The big class of layered ternary carbide and/or nitride has various good properties such as low density, high thermal and electrical conductivity, excellent thermal shock, exceptional oxidation resistance, high elastic modulus, damage tolerance and easy machinability characteristics.[2,3] Due to these properties, especially the excellent tolerance to irradiation damage, MAX phases have been considered as potential fuel coatings and cladding materials used in core components of future gas-cooled fast nuclear reactors and fusion programs.[4]

In face of the long-term operation in extreme environments of elevated temperatures (> 1000 °C) and severe radiation fluences as high as 150 dpa–200 dpa (displacement per atom), the damage tolerance of the MAX phase is of vital importance for applications in future nuclear systems. Previous studies show that $M_{n+1}AX_n$ can accommodate radiation-induced point defects with low formation energy and the easier formation of M_A–A_M (an atom replaced by an M atom and an M atom replaced by an atom) antisite pairs provides an alternative way to accommodate the defects.[5,6] Nevertheless, various MAX materials behave differently in the ion radiation experiments. Some MAX phases can be rendered amorphous easily, whereas others show little loss of crystallinity even at very high radiation doses. The Ti_3AlC_2 is found to be more radiation-resistant than Ti_3SiC_2. The Ti_3AlC_2 remains crystalline at ~25 dpa under the radiation of 1-MeV Xe, whereas Ti_3SiC_2 turns amorphous under the same condition.[7] Two of the most radiation damage-tolerant materials theoretically, Ti_2AlC and Ti_2AlN,[8] have been investigated for their radiation tolerance in experiments by Ar^{2+} ion and neutron irradiation. The experiments showed that both of them withstand 100-keV Ar^{2+} ion irradiation and 0.1dpa of neutron radiation.[9,10] The experiments also demonstrated a major difference in amorphization between Cr and Ti-based MAX phases: the Cr-based MAX phase has a much lower amorphization threshold dose than Ti-based MAX phases.[8] Meanwhile, Cr_2AlC is more tolerant than Cr_2GeC under the radiation of 340-keV Xe: Cr_2GeC becomes fully amorphous at ~ 0.8 dpa, whereas Cr_2AlC becomes amorphous at ~ 2 dpa.[11] Since there are tens of MAX species, it takes time and expense-consuming if we test all these materials experimentally, thus it becomes important to analyze their irradiation tolerance mechanism. The current experimental data are far

*Project supported by the National Natural Science Foundation of China (Grant Nos. 91226202 and 91426304).
†These authors contributed equally to this work
‡Corresponding author. E-mail: jmxue@pku.edu.cn
© 2017 Chinese Physical Society and IOP Publishing Ltd

from enough to set up a criterion to distinguish MAX phases with better irradiation tolerance from the others. Therefore, it is critical to develop a theoretical method of choosing the most prospective sample for the experiment.

When materials are subjected to neutron or ion irradiations, the target atom will be dislodged from its lattice site after receiving sufficient energy, and then further collide with other target atoms, creating a displacement cascade. The cascade can be either quenched into a nanometer-scaled amorphous domain or annealed quickly with some point defects consisting of vacancies, interstitials, antisite defects, or defect clusters.[7,12] During the past few decades, many criteria have been proposed to explain the stability of ceramics under irradiation such as the geometrical structure, melting point, polymerization index, elastic modulus, and bonding type.[13] Among these models, the bonding type was proposed as a factor relating resistance to amorphization for the first time by Naguib and Kelly in 1975,[13] and then it was discussed in detail in Trachenko *et al.*'s[14] work and was proved to be a key parameter to control the response of material to irradiation damage. It is supposed that the ability to resisting the irradiation is generally governed by the competition between the short-range covalent force and long-range ionic force.[14,15] A complex material is readily amorphizable by radiation damage if it is able to form a covalent network. This method has been successfully used to explain the different radiation resistances of 116 materials that are different from their families, including binary and ternary compounds. The advantage of this model is that it can be applied extensively to compounds with different compositions and chemical structures.

In this paper, we present a comprehensive study on the properties of various charge states based on the Bader analysis[16] and the first-principle calculation.[17] We quantify the proposed theory of resistance to amorphization from the electronic structures in several pairs of MAX phase materials. Furthermore, we propose to use the effective charge transfer as an independent criterion to elucidate the amorphization mechanism. Our calculations accord with the experimental results, showing that it is reliable and accurate. Our method possesses the value of practical applications since it may achieve unified cognition of $M_{n+1}AX_n$ material behaviors under neutron and ion irradiations.

2. Method of calculation

First-principle calculations were conducted with the Vienna Ab initio simulation package (VASP).[18,19] The frozen-core projector augmented-wave (PAW)[20,21] potentials were used to describe the interaction between ions and electrons. The generalized gradient approximation (GGA-PBE) is used for treating the electronic exchange-correlation function. In the meantime, Bader analysis, a novel method, is used to calculate the effective charge on individual atoms. Being an intuitive scheme for visualizing atoms in molecules, Bader's definition makes use of so-called zero flux surfaces to divide atoms. Bader analysis is better than wave function-based population methods (e.g., Mulliken population analysis)[22] because it is based on the charge density, which is an observable quantity that can be measured experimentally or calculated. Furthermore, the charge density is insensitive to the basis set used. Also, it carries out decomposition of electronic charge density into atomic contributions. The charge enclosed within the Bader volume is a good approximation to the total electronic charge of an atom.[16] Together with the VASP code, it was used to quantify the core charge and partition electrons amongst fragments of the system in MAX phases.

In the detailed calculation settings, the total energy was converged to better than 0.1 meV with a plane wave cutoff of 450 eV. The density of states (DOS) calculation was based on a primitive unit cell and Brillouin zone sampling was performed by using the Monkhost–Pack scheme with a k-point grid of $21\times21\times21$, whereas a small Monkhorst–Pack $8\times8\times4$ k-point sampling for the Brillouin zone was used in a static self-consistent calculation.[23] The values of the kinetic energy cutoff and the k-point grid were determined by the convergence of total energies. All calculations were performed within a primitive unit cell containing 12 atoms and 8 atoms, respectively for M_3AC_2 and M_2AC structures. The method of conjugate gradient energy minimization was used for geometry relaxation. The lattice vectors of the cell and all the atoms were allowed to relax until atomic forces were less than 0.01 eV/Å.

3. Results and discussion

3.1. Structural properties of $M_{n+1}AX_n$

The MAX phases have a hexagonal symmetry in space group $P63/mmc$ with Wyckoff positions. The structure of 312 MAX phases consists of hexagonal layers stacked in the repeated sequence A–$M(1)$–X–$M(2)$–X–$M(1)$. There are two non-equivalent M atoms denoting $M(1)$ and $M(2)$ with Wyckoff positions of $4f$ (1/3, 2/3, z_{M1}) and $2a$ (0,0, 0), respectively. The A plane atoms are located in $2b$ (0, 0, 1/4) and X atoms in $4f$ (1/3, 2/3, z_X).[24] Analogously, the isomorphous structure of 211 MAX phases consists of a repeated atomic layer sequence of A–M–X–M. The M_6X octahedra, similar to those formed in respective MX binary carbides, are connected with each other by shared edges. The main difference in structure between 211 and 312 phases lies in the number of M layers in between every two A layers.

We perform a thorough research with 12 MAX phases (Ti_3SiC_2, Ti_3AlC_2, Ti_3SiN_2, Ti_3AlN_2, Cr_2AlC, Cr_2GeC, Cr_2GaC, Nb_2AlC, Ta_2AlC, Ti_2AlC, Ti_2AlN, and V_2AlC), most of which have been previously investigated experimentally. We first calculate the lattice constants of these MAX

phases to validate both the pseudopotentials and the method used in this simulation. The calculated structural parameters are shown in Table 1. The calculated lattice parameters of a, c values from experiments and previous calculations are also included for comparison. The values in a/b–Err (%) and c–Err (%) denote the percentage differences among lattice parameters between the calculated values and experimental data, respectively. Some of the blanks in this table represent that they have not been synthesized experimentally yet or they have not been calculated with the DFT method before. As we can see, the lattice parameters in our calculation are similar to the experimental data, while the slight differences between different theoretical calculations can be reasonably attributed to the GGA function used. The results validate our method.

Table 1. The lattice parameters (in unit of Å) for Ti_3SiC_2, Ti_3AlC_2, Ti_3SiN_2, Ti_3AlN_2, Cr_2AlC, Cr_2GeC, Ti_2AlC, Ti_2AlN, and V_2AlC; a/b–Err (%) and c–Err (%) denote the largest percentage differences among lattice parameters between the calculated values and experimental data.

Composition		a/b	c	a/b–Err (%)	c–Err (%)
Ti_3SiC_2	this work	3.075	17.708	0.26	0.209
	DFT[6]	3.077	17.706	0.32	0.198
	EXP[25]	3.067	17.671		
Ti_3AlC_2	this work	3.082	18.641	0.032	0.833
	DFT[6]	3.081	18.594	0	0.578
	EXP[25]	3.081	18.487		
Ti_3SiN_2	this work	2.983	17.826		
	DFT[26]	2.99	17.84		
	EXP				
Ti_3AlN_2	this work	3.002	18.463		
	DFT[26]	3.00	18.49		
	EXP				
Cr_2AlC	this work	2.844	12.685	–0.663	–1.0
	DFT[22]	2.842	12.687	–0.733	–0.991
	EXP[25]	2.863	12.814		
Cr_2GeC	this work	2.938	12.024	–0.406	0
	DFT [22]	2.925	12.024	–0.847	0
	EXP	2.95	12.024		
Cr_2GaC	this work	2.87	12.54	–0.347	0.555
	DFT				
	EXP[27]	2.88	12.61		
Ti_2AlC	this work	3.068	13.731	0.557	0.689
	DFT[28]	3.04	13.60	–0.36	–0.271
	EXP[25]	3.051	13.637		
Ti_2AlN	this work	2.993	13.614	0.133	0
	DFT[29]	2.99	13.61	0.033	0.03
	EXP[22]	2.989	13.614		
V_2AlC	this work	2.905	13.118	0.239	0.167
	DFT[27]	2.91	13.13	0.068	0.0761
	EXP[24]	2.912	13.140		

3.2. Bonding characters

The MAX phases can be considered as robust materials when subjected to ion irradiation. Nevertheless, according to observations different MAX phases behave differently under irradiation and the reason for this remains unclear. Motivated by the necessity to focus extensively on the evolution of the microstructure during the irradiation, we summarize some experimental data to illustrate the diversity of radiation tolerance, and the results are given in Table 2.

Basically, all the macroscopic properties of materials originate from their electronic structure properties as well as the natures of the chemical bonding. Trachenko *et al*. have given a more general comprehension of the physics of radiation damage.[14] A material with high ionic bonding is more resistant to amorphization than a material with covalent bonding. In general, short-range covalent contributions lead to highly directional bonds and a number of distinct potential energy minima which act as barriers to recovery of periodicity in the vicinity of the collision cascade, whereas long-range ionic contributions minimizes the barriers to recovery of atomic periodicity. What is more, the local recrystallization process is promoted in a material with high ionicity of bonding by ions attracting oppositely charged neighbors and making the "defect" structures that consist of neighboring atoms of the same charge energetically unfavorable, whereas this effect is absent in a covalent structure.[13,15]

Based on the model provided by Trachenko, the relations between radiation resistance and the bonding trend of these MAX phases can be further analyzed by the calculated total electron density of states (TDOS) as well as their partial density of states (PDOS) as demonstrated in Figs. 1 and 3. The DOS at Fermi level (E_F) determines the electronic conductivity characteristics and all of the MAX phases we calculated are finite at the Fermi energy level, which indicates the metallic properties of MAX phases. What is more, there is a high degree of hybridization of M orbitals and X orbitals, suggesting a strong covalent interaction between M–X in the material. The position of the E_F in TDOS reveals the stability of the system while a local minimum represents relative stablility. As for Ti_3AlC_2, Ti_3AlN_2, Cr_2AlC, Ti_2AlC, V_2AlC, Ta_2AlC, Nb_2AlC, Cr_2GaC, and Ti_2AlN, the TDOS around the Fermi level is at a local minimum in contrast to that of Ti_3SiC2, Ti_3SiN_2, and Cr_2GeC. The conduction bands above E_F are composed mainly of the M atom states. The dose below E_F contains mainly 3s and 2s states contributed by A and X atoms, respectively. The increase in N (E_F) tends to coincide with the increase in valence electrons of the corresponding element.[24]

To illustrate the influence of transition metal M in MAX phase in terms of its radiation resistance observed in experiment, we choose Ti_2AlC, Cr_2AlC, and V_2AlC for investigating the relations between their radiation resistance and bonding trend. The DOS and PDOS of them are presented in Fig. 3. There is no obvious difference in PDOS of the C atom among these three MAX phases, but a distinct difference can be seen from the hybridizations of M_d–Al_p in Cr_2AlC, V_2AlC, and Ti_2AlC. The hybridization of Ti–Al in Ti_2AlC is closer to E_F than that of V–Al in V_2AlC, while hybridization of Cr–Al in Cr_2AlC is farthest to E_F. This difference possibly originates from the fact that the Ti atom has one less charge elec-

tron than V, and the V atom has one less charge electron than Cr. The weaker bonding of Ti–Al behaves more like an ionic bond which allows the damaged structure to reestablish coherence with the crystalline lattice more easily, whereas the structural reconstruction with stronger bondings of V–Al and Cr–Al should require additional energy cost.

Table 2. Summarized experimental data concerning the radiation tolerances of the six $M_{n+1}AX_n$ materials: Ti3AlC2, Ti3SiC2, Ti2AlC, Ti2AlN, Cr2GeC, and Cr2AlC. Different experimental conditions and variables are shown below (RT denotes room temperature).

Incident ion	MAX material	Fluences/cm^{-2}	Temperature/°C	dpa	Degree of amorphization
1-MeV Xe[7]	Ti_3AlC_2	3.25×10^{14}	RT		no amorphization
	Ti_3SiC_2	3.25×10^{14}	RT		begin amorphous
neutron(>0.1 MeV)[10]	Ti_2AlC	4.00×10^{20}	360($\pm$20)	0.1	decompose into TiC from the pristine 6.7% to 8.3%
		4.00×10^{20}	695($\pm$25)	0.1	decompose into TiC from the pristine 6.7% to 4.3%
	Ti_2AlN	4.00×10^{20}	360($\pm$20)	0.1	decompose into TiN from the pristine 3.23% to 11.6%
		4.00×10^{20}	695($\pm$25)	0.1	decompose into TiN from the pristine 3.23% to 13%
	Ti_3AlC_2	4.00×10^{20}	360($\pm$20)	0.1	decompose into TiC from the pristine 1.9% to 52.6%
		4.00×10^{20}	695($\pm$25)	0.1	decompose into TiC from the pristine 1.9% to 44.4%
	Ti_3AlN_2 (fine - grained)	4.00×10^{20}	360($\pm$20)	0.1	decompose into TiN from the pristine 20% to 22.7%
		4.00×10^{20}	695($\pm$25)	0.1	decompose into TiN from the pristine 20% to 25%
1-MeV Au[30]	Ti_2AlC	1.00×10^{14}	RT		no amorphization
		3.00×10^{14}	RT		no amorphization, begin to emerge stacking faults
		1.00×10^{16}	RT		partial phase transition from hcp to fcc
		2.00×10^{16}	RT		entirely transformed into the fcc phase
100-keV Ar[9]	Ti_2AlN	1.8×10^{13}–1.3×10^{15}	RT	up to 12	no amorphization
320-keV Xe[11]	Cr_2GeC	5.00×10^{13}	RT	0.41	begin amorphous
		1.00×10^{14}	RT	0.82	fully amorphous
	Cr_2AlC	1.00×10^{14}	RT	0.62	no amorphization
		3.50×10^{14}	RT	2.2	begin amorphous
		6.00×10^{14}	RT	3.7	fully amorphous
		1.00×10^{15}	RT	6.2	fully amorphous

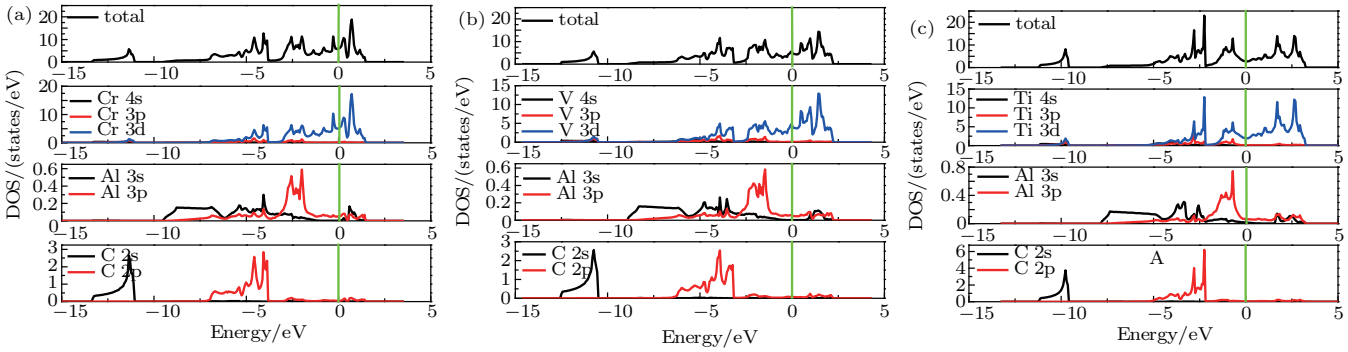


Fig. 1. (color online) Calculated energy-dependent densities of states and partial densities of states for (a) Cr_2AlC, (b) V_2AlC, and (c) Ti_2AlC, where the green line represents DOS at Fermi level.

Regarding the bonding trend between *M* and *A*, the various resistances to amorphization of Ti_2AlC, V_2AlC, and Cr_2AlC under the same irradiation condition can be easily explained. The weak interaction of *M*–*A* in MAX phase promotes irradiated defects recombination, which contributes to preserving their crystalline structures. So the substitutions of Cr by V and V with Ti can increase the resistance of radiation, leading to the conclusion that the crystal structure of the Ti-based M_2AX phase is more resistant to amorphization of radiation than that of the V-based M_2AX phase, and so is the case of V-based M_2AX phases to Cr-based M_2AX phases.

The charge density contours can also be used to explain the differences in bonding characters. We expand our ideas to the *M*–*A* bonding character in the context of the calculated charge density. It is suggested that the high radiation damage tolerance exhibited by many ceramic *M*–*X* compounds and the rapid recovery from damage which is inherent in metallic *M*–*A* compounds are both present in MAX phases. Figure 2 shows the charge density contours on the (1120) plane for (a) Cr_2AlC, (b) V_2AlC, and (c) Ti_2AlC. One can clearly observe the polarization of the electronic charge around the *M* atoms which points toward the C atoms in the center. The charge around the C atom is non-spherical, consistent with the existence of covalent bonds between *M* and C. The charge densities around *X* atoms are obviously greater than those around A atoms, demonstrating the stronger covalent bonding between *M* and *X*. The coupling between *M*–C and *M*–Al shows a declining trend for each of Cr_2AlC, V_2AlC, and Ti_2AlC, il-

lustrating that a strong covalent bonding is formed between Cr–C, whereas the bonding around Ti turns more ionic. The stronger bondings of *M*–*X* and *M*–*A* in Cr-based M_2AX phases than in Ti-based M_2AX phases exhibit that they have lower radiation tolerances. The charge density contours we calculated are consistent with the DOS we simulated and also with the experiment results.

A similar method has also been used in Xiao *et al.*'s work,[8] in which this model was validated. Our discussion also verifies the theory on the relationship between irradiation resistance and bonding type. To provide the further comprehension of the mechanism, much more atoms are tested.

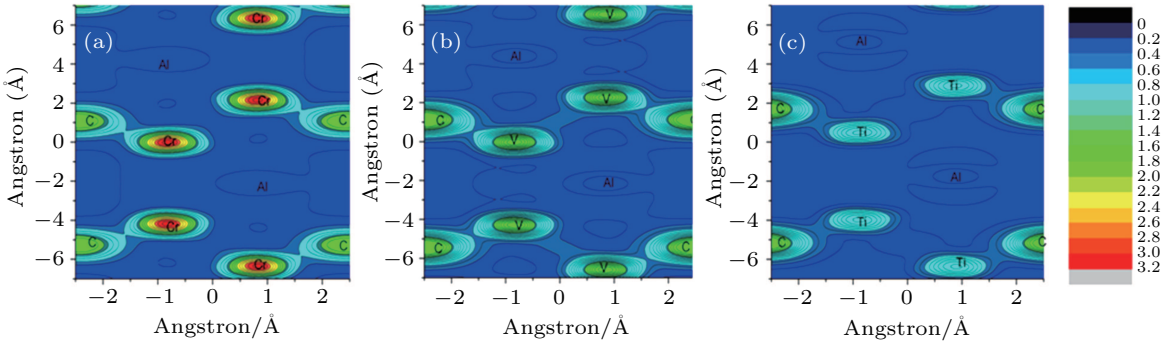


Fig. 2. (color online) Distributions of electron charge density on the (1120) plane for (a) Cr_2AlC, (b) V_2AlC, and (c) Ti_2AlC, where charge density varies from 0.1 (blue) to 3.2 e/Å^3 (dark red).

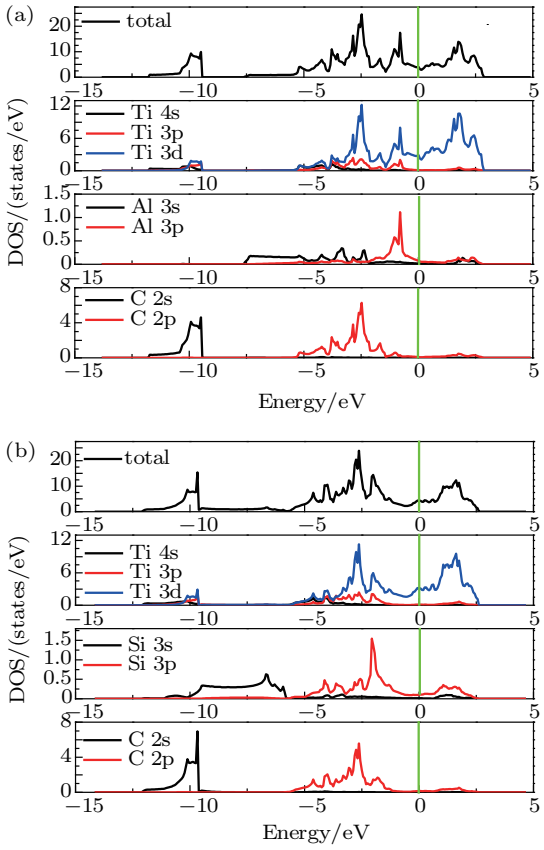


Fig. 3. (color online) Calculated energy-dependent densities of states and partial densities of states for (a) Ti_3AlC_2 and (b) Ti_3SiC_2. The green line indicates DOS at Fermi level.

An atom in MAX phases also plays a major role in radiation resistance.[31] To elucidate the different behaviors of *A* atoms when subjected to the radiation of energetic ions, we focus on the bonding characters of two structures: Ti_3AlC_2 and Ti_3SiC_2. The TDOS and PDOS of them are shown in Fig. 3. Each of Ti_3SiC_2 and Ti_3AlC_2 has a high degree of hybridization between Ti 3d orbitals and C 2p orbitals, indicating a strong covalent interaction between Ti-C in these two materials. The hybridization of Ti–Al in Ti_3AlC_2 is much closer to E_F than that of Ti–Si in Ti_3SiC_2, revealing that the bonding between Ti–Al is weaker than Ti–Si.

It can be further verified by the directional bonds between Ti-Si and Ti–Al in these two compounds as revealed by the electron density distribution plot demonstrated in Fig. 4. There are strong covalent bonds between Ti and C atoms, forming directional Ti–C bond chains. The density located in the Ti–Al region is much smaller than that in Ti–Si. The weaker bonding of Ti–Al behaves more like an ionic bond, which represents higher radiation tolerance, while the stronger bonding of Ti–Si shows lower tolerance. There are also some notable differences in bonding between *A* and *X*. It should be noted that there are some strong peaks at the same energy in the PDOS of some particular Si atoms and C atoms. A considerable overlap between C 2s, C 2p, Si 3s, and Si 3p orbitals shows a strong covalent bonding, while there is no significant overlap between the C 2s and C 2p orbitals with the Al 3s and Al 3p orbitals in Ti_3AlC_2. The weak overlap between Al and C denotes that minimal interaction is likely to exist between these two elements, primarily due to the difference in energy. The interaction between Si–C is much stronger than that between Al–C in these two MAX phases, leading to different recovery processes subjected to ion irradiation. Because of the notable overlap between Si and C, it is more likely to form nanoscale SiC[32] rather than Ti_3AlC_2 in the recovery recrystallization process. The weaker bonding between Al and C in Ti_3AlC_2 is more likely to form point defects such as antisite defects and Frenkel pairs which increase the possibility to recombine into a crystalline structure. All the calculated results are consistent with our experimental data, validating the universality of our simulations.

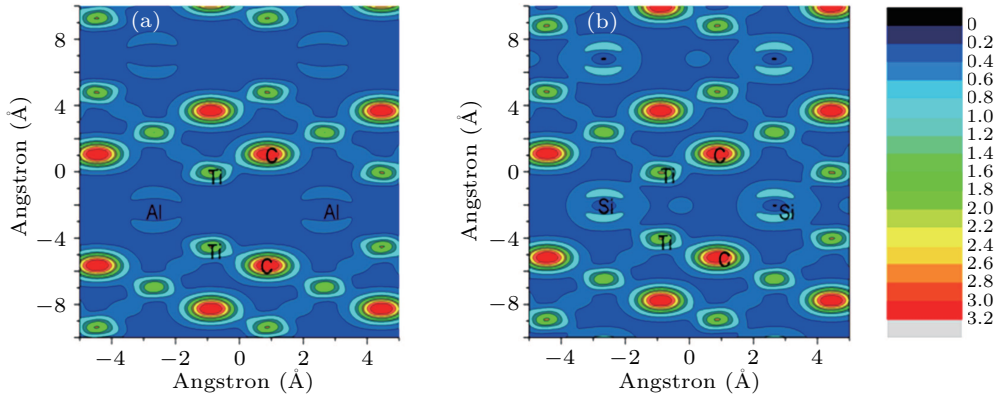


Fig. 4. (color online) Distributions of electron charge density of (a) Ti_3AlC_2 and (b) Ti_3SiC_2, where charge density varies from 0.1 (blue) to 1.7 e/Å ^{3} (dark red).

This can also explain the greater resistance to amorphization of Cr_2AlC than Cr_2GeC under the same irradiation condition. The structural reconstruction with stronger bonding of Cr–Ge than Cr–Al should require additional energy cost, which leads to low radiation tolerance.

The improved radiation tolerance of Ti_2AlC compared with Ti_3AlC_2 observed in the experiments has drawn a great deal of attention in recent years. Rietveld analyses of the XRD spectra for Ti_2AlC and Ti_3AlC_2 revealed a drastic difference in irradiation tolerance between the two compounds in Tallman *et al.*'s work.[10] By enhancing the inherent ability to accommodate radiation-induced defects in nanostructured composites, the A atomic plane is supposed to play a decisive role in improving the radiation tolerance of the material.[31] In terms of the same chemical elements, other factors should be introduced to fully explain the improvements of radiation tolerance. We focuse on the increased ratio of the Al/TiC layer and the relative interlayer distance in lattice. The density of A atomic planes grows with the increase of the Al/TiC layer. The interlayer distance between Ti–C–Ti in Ti_2AlC is almost half that in Ti_3AlC_2, indicating that Ti_2AlC has more intercalated A atomic planes per MX layer than Ti_3AlC_2. From this perspective, we can explain the improvement of radiation tolerance from Ti_3AlC_2 to Ti_2AlC observed in experiments.

By making a comparison of DOS and charge density among different MAX phases, we find that crystal-structured Ti-based MAX phases are more resistant to amorphization than V/Cr-based MAX phases, and the $M_{n+1}AlX_n$ phases are more resistant than $M_{n+1}SiX_n$ phases. In conclusion, the substitution of Si by Al and Cr/V by Ti introduce extra valence electrons into each atom, improving the resistance to amorphization. The difference in dominating M_d/A_p hybridization between $M_{n+1}AC_n$ and $M_{n+1}AN_n$ is not obvious, which means that they have similar resistances.

3.3. Charge characters

Though the irradiation tolerance of the MAX phase could be roughly estimated by analyzing its DOS and charge density map and so on, it is still difficult to compare more than three MAX phases. It is also difficult to obtain a conclusion by using the density of electron in a certain surface. It should depend on the three-dimensonal (3D) distribution of electrons. Therefore, we try to use the effective charge as a new tool and it is generally perceived to be more accurate than bonding characters presented by DOS overlap and visual observation of the charge density map.[8,24]

The criterion in terms of charge is based on the good empirical correlation of resistance with the ionicity of the chemical bond, using Pauling or Phillips definitions.[33] It should be noted that neither of the concepts of 'ionicity' and 'covalency' is clearly defined because both of them contribute considerably to a bond, making it impossible to draw a clear line between them. One of the reliable ways to determine the bonding character is to analyze the electron density maps obtained from either experimental diffraction methods or quantum-mechanical calculations. Unlike the Bader analysis method in our research, the Voronoi deformation density charges[34] and Mulliken overlap population[35,36] were calculated in Trachenko *et al.*'s work. In their report, they proposed that the increase of Q and decrease of M result in the increase of resistance of a complex compound.[14] But it is not obvious to attribute the charges to one atom or the other in Mulliken overlap population, which is based on the plane wave basis. According to the above discussion, we choose the Bader analysis because it is intuitive to calculating the charge in individual atoms in molecules and crystals, and it also conforms to chemical experience. We have recently compiled the list of twelve materials to illustrate that their resistances can be generally explained by charge transfer as shown in Figs. 5 and 6. The bonding type and charge transfer values of these different 312 and 211 MAX phases are analyzed for allowing the comparison among them.

The amount of charge transfer can characterize the degree of ionicity in a certain MAX-phase compound. The bond behaves more like an ionic bond when the charge transfer value is a high positive or low negative value, allowing the damaged

structure to reestablish coherence with the crystalline lattice more easily, whereas the low positive or high negative charge transfer behaves more like a covalent bond, which should require additional energy cost in structural reconstruction.[37] In this case, we make an in-depth analysis on charge transfers of different M, A, and X atoms in MAX phases.

Regarding the charge transfer trend with 211 MAX phases, M elements have significant influences on the irradiation damage process. From Fig. 5, it can follow that the transition-metal atoms always lose charges. The calculations show that the charge transfers on M atoms decrease in the sequence of Ti_2AlC, V_2AlC, and Cr_2AlC. The charge transfer of Cr in Cr_2AlC is 0.5011, indicating that it loses 0.5011 electrons and V in V_2AlC loses 0.8692 electrons and Ti in Ti_2AlC loses 1.1903 electrons. The higher charge transfer value for early transition metal represents higher ionicity and reduced barriers to regain coherence with the crystalline lattice which makes them significantly more resistant to amorphization. Our predictions of the contrasting stability are also inconsistent with the experimental results. We also calculate the other two M atoms whose radiation tolerance has not been tested in experiment. Nb in Nb_2AlC and Ta in Ta_2AlC lose 0.9040 and 0.9699 electrons respectively. According to our calculated charge transfer of M atoms, we can make a prediction that the crystal-structured Ti-based MAX phase materials are more resistant to amorphization than other materials with the same A and X atoms.

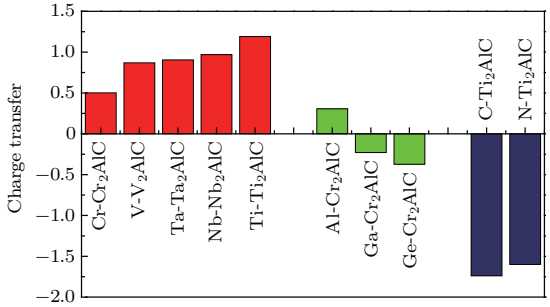


Fig. 5. (color online) Charge transfer values of different atoms in different 211 MAX phases, illustrating the discussion about the resistance to amorphization. The red column denotes charge transfer of the M atom in M_2AlC, the green column refers to charge transfer of the A atom in Cr_2AC, while the blue column represents charge transfer of the X atom in Ti_2AlX. A positive value shows that they lose electrons, whereas the negative value denotes that they gain electrons.

The charge transfer of A atoms in MAX phases plays an important role in their resisting amorphization. The intercalated A atoms in the nanolaminated crystal $M_{n+1}AX_n$ promote the accommodation of disordering defects within their structures by enhancing the inherent ability to accommodate radiation-induced defects. So we further study the significant difference in radiation tolerance between Cr_2GeC, Cr_2GaC, and Cr_2AlC in 211 MAX phases. It is noted that Al in Cr_2AlC loses 0.3063 electrons, whereas Ga in Cr_2GaC obtains 0.2296 electrons and Ge in Cr_2GeC gains 0.3727 electrons. That is to say, the bonding around Ge in Cr_2GeC behaves as being more covalent than those of the bonding around Ga in Cr_2GaC and Al in Cr_2AlC, conducive to its chemistry forming a covalent network. As a result, an additional energy is required to break the strong covalent bond, inducing the radiation tolerance of Cr_2GeC to be lower than those of Cr_2GaC and Cr_2AlC. Though there are no experimental data about irradiation for Cr_2GaC, we can theoretically predict that it is not the most promising candidate for the nuclear system.

Finally, we focus on the effects of X atoms on radiation tolerance of 211 MAX phases. In Ti_2AlC, the charge transfer value of C is slightly lower than that of N in Ti_2AlN, while C obtains 1.7389 electrons and N gains 1.6 electrons. The similar charge transfer value manifests the basically consistent radiation tolerance of them and no quantitative description of their differences has been shown experimentally so far.

The mechanism of amorphization in terms of the bonding characters in these 211 MAX phases demonstrates that the substitution of Ge/V/Ta/Nb by Ti and Si/Ga by Al in M_2AX phases induces higher radiation resistance because the bonds behave as being more ionic. That is to say, as the weight of the short-range covalent forces goes down and the weight of long-range ionic forces goes up, its resistance increases.

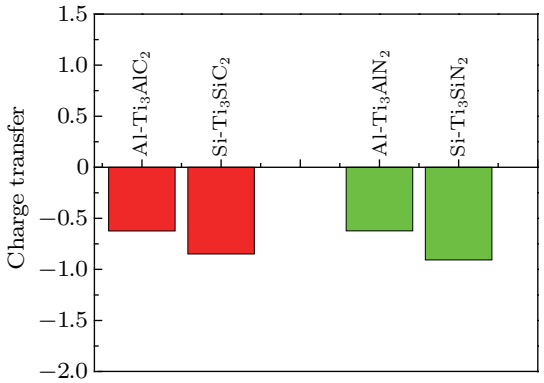


Fig. 6. (color online) Charge transfer values of different atoms in different 312 MAX phases, illustrating the discussion about the resistance to amorphization.

A meaningful comparison of the character of charge transfer electrons among 312 MAX phases can also be carried out. Our calculation about charge transfer contrasts the result from the readily amorphizable materials with resisting the radiation. It is illustrated that the Si in Ti_3SiC_2 and Ti_3SiN_2 obtain more electrons than Al in Ti_3AlC_2 and Ti_3AlN_2 as shown in Fig. 6. The increase of positive charge transfer value and decrease of negative charge transfer value improve the radiation tolerance of 312 MAX phases. Thus, the covalent bonding character of elemental Si in Ti_3SiC_2 and Ti_3SiN_2 lower the resistances to amorphization compared with the scenario of Al in Ti_3AlC_2 and Ti_3AlN_2.

Covalency and ionicity are different characterization ways in which the electron density can be distributed in a solid. Higher ionicity promotes the recombination of irradiated defects, contributing to preserving their crystalline structure. The difference in charge transfer between different atoms in MAX phases can explain the diversity of resistance to amorphization under the same irradiation condition, and also leads to a prior consideration of selecting the MAX phases that can highly resist the radiation for the applications in a future nuclear system.

4. Conclusion and perspectives

The charge transfers of 312 and 211MAX phases are investigated based on the Bader analysis method. We quantify the proposed theory of resistance to amorphization from the electronic structure of each atom. The interatomic *M*–*X*, *M*–*A*, and *X*–*A* bonding characters are also analyzed to further illustrate the radiation damage mechanisms in these $M_{n+1}AX_n$ materials. The competing effect between the short-range covalent and long-range ionic forces demonstrates that a complex material can be readily amorphized by radiation damage if its chemistry allows it to form a covalent network. The increase (decrease) of the short-range covalent component in the total force field of material reduces (increases) its resistance. Our results demonstrate that for the *M* atoms, Cr/V/Ta/Nb-based MAX phases are more amorphizable than Ti-based MAX phases. For the intercalated *A* atoms, the substitution of Si/Ga/Ge by Al will gain higher resistance. The weaker bonding of Ti–Al behaves more like an ionic bond, allowing the damaged structure to reestablish coherence with the crystalline lattice more easily, whereas the reconstruction of stronger bonding of Ti–Si and Cr–Al/Cr–Ge/ Cr–Ga should require additional energy. As for the 312 and 211 structures with the same chemical elements, the *A* atomic plane in the nanolaminated crystal $M_{n+1}AX_n$ can accommodate radiation-induced point defects. The increased ratio of the A/MX layer and the relatively low interlayer distance in the lattice indicate that 211 MAX phases can be more resistant to radiation than 312 MAX phases. Our calculations show a possibility that the values of resistance to amorphization for these materials can be predicted by analyzing the corresponding charge transfer values and bonding characters, offering a criterion for selecting an appropriate MAX phase used in an irradiation environment to further experiment on irradiation. Our results suggest that Ti_2AlC and Ti_2AlN are two of the most promising MAX phase materials in application.

Acknowledgment

The authors thank the National supercomputer center in GUANGZHOU for providing computing resources.

References

[1] Barsoum M W 2000 *Prog. Solid State Chem.* **28** 201
[2] Barsoum M W, El-Raghy T, Rawn C J, Porter W D, Wang H, Payzant E A and Hubbard C R 1999 *J. Phys. Chem. Solids* **60** 429
[3] Radhakrishnan R, Williams J J and Akinc M 1999 *J. Alloys Compd.* **285** 85
[4] Nappé J C, Grosseau P, Audubert F, Guilhot B, Beauvy M, Benabdesselam M, and Monnet I 2009 *J. Nucl. Mater.* **385** 304
[5] Middleburgh S C, Lumpkin G R, Riley D and Zhon Y 2013 *J. Am. Ceram. Soc.* **96** 3196
[6] Zhao S, Xue J, Wang Y and Huang Q 2014 *J. Appl. Phys.* **115** 023503
[7] Whittle K R, Blackford M G, Aughterson R D, Moricca S, Lumpkin G R, Riley D P and Zaluzec N J 2010 *Acta Mater.* **58** 4362
[8] Xiao J, Yang T, Wang C, Xue J, Wang Y and Sinnott S 2015 *J. Am. Ceram. Soc.* **98** 1323
[9] Bugnet M, Cabioc'h T, Mauchamp V, Guérin P, Marteau M and Jaouen M 2010 *J. Mater. Sci.* **45** 5547
[10] Tallman D J, Hoffman E N, Caspi E a N, Garcia-Diaz B L, Kohse G, Sindelar R L and Barsoum M W 2015 *Acta Mater.* **85** 132
[11] Bugnet M, Mauchamp V, Oliviero E, Jaouen M and Cabioc'h T 2013 *J. Nucl. Mater.* **441** 133
[12] Nappé J C, Monnet I, Grosseau P, Audubert F, Guilhot B, Beauvy M, Benabdesselam M and Thomé L 2011 *J. Nucl. Mater.* **409** 53
[13] Trachenko K 2004 *J. Phys.: Condens. Matter* **16** R1491
[14] Trachenko K, Pruneda J M, Artacho E and Dove M T 2005 *Phys. Rev. B* **71** 184104
[15] Trachenko K, Dove M T, Artacho E, Todorov I T and Smith W 2006 *Phys. Rev. B* **73** 174207
[16] Tang W, Sanville E and Henkelman G 2009 *J. Phys.: Condens. Matter* **21** 084204
[17] Kresse G and Furthmüller J 1996 *Comput. Mater. Sci.* **6** 15
[18] Hohenberg P and Kohn W 1964 *Phys. Rev.* **136** B864
[19] Kresse G and Furthmüller J 1996 *Phys. Rev. B* **54** 11169
[20] Blöchl P E 1994 *Phys. Rev. B* **50** 17953
[21] Kresse G and Joubert D 1999 *Phys. Rev. B* **59** 1758
[22] Li N, Mo Y X and Ching W Y 2013 *J. Appl. Phys.* **114** 023708
[23] Monkhorst H J and Pack J D 1976 *Phys. Rev. B* **13** 5188
[24] Mo Y, Rulis P and Ching W Y 2012 *Phys. Rev. B* **86** 165122
[25] Sun Z M 2011 *Int. Mater. Rev.* **56** 143
[26] Keast V J, Harris S and Smith D K 2009 *Phys. Rev. B* **80** 214113
[27] Barsoum M W and Radovic M 2011 *Ann. Rev. Mater. Res.* **41** 195
[28] Zhou Y C and Sun Z M 2000 *Phys. Rev. B* **61** 12570
[29] Sickafus K E, Minervini L, Grimes R W, Valdez J A, Ishimaru M, Li F, McClellan K J and Hartmann T 2000 *Science* **289** 748
[30] Wang C, Yang T, Xiao J, Liu S, Xue J, Wang J, Huang Q and Wang Y 2015 *Acta Materialia* **98** 197
[31] Sickafus K E, Grimes R W, Valdez J A, Cleave A, Tang M, Ishimaru M, Corish S M, Stanek C R and Uberuaga B P 2007 *Nat. Mater.* **6** 217
[32] Lucas G and Pizzagalli L 2007 *Nucl. Instrum. Methods Phys. Res. B* **255** 124
[33] Phillips J C 1970 *Rev. Mod. Phys.* **42** 317
[34] Fonseca Guerra C, Handgraaf J W, Baerends E J and Bickelhaupt F M 2004 *J. Comput. Chem.* **25** 189
[35] Li X H, Zhu L G and Yu Q S 2000 *Chem. J. Chin. Univer.* **21** 1118
[36] Mulliken R S 1955 *J. Chem. Phys.* **23** 1841
[37] Latimer W M 1951 *Science* **113** 253